PFMC-15

Thermal shock behaviour of H and H/He-exposed tungsten at high temperature

N Lemahieu[1,2,3], H Greuner[4], J Linke[1], H Maier[4], G Pintsuk[1], M Wirtz[1], G Van Oost[2] and J-M Noterdaeme[2,4]

[1] Forschungszentrum Jülich GmbH, Institut für Energie- und Klimaforschung, 52425 Jülich, Germany

[2] Department of Applied Physics, Ghent University, St.-Pietersnieuwstraat 41 B4, 9000 Ghent, Belgium

[3] Institute of Interfacial Process Engineering and Plasma Technology IGVP, Universität Stuttgart, Pfaffenwaldring 31, 70569 Stuttgart, Germany

[4] Max-Planck-Institut für Plasmaphysik, Boltzmannstraße 2, 85748 Garching, Germany

E-mail: `n.lemahieu@fz-juelich.de`

Abstract. Polycrystalline tungsten samples were characterized and exposed to a pure H beam or mixed H/He beam containing 6% He in GLADIS at a surface temperature of 600°C, 1000°C, or 1500°C. After 5400 s of exposure time with a heat flux of 10.5 MW/m^2, the total accumulated fluence of 2×10^{25} m^{-2} was reached. Thereafter, ELM-like thermal shocks with a duration of 1 ms and an absorbed power density of 190 MW/m^2 and 380 MW/m^2 were applied on the samples in JUDITH 1. During the thermal shocks, the base temperature was kept at 1000°C. The ELM-experiments with the lowest transient power density did not result in any detected damage. The other tests showed the beginning of crack formation for every sample, except the sample pre-exposed with the pure H-beam at 1500°C in GLADIS. This sample was roughened, but did not show any crack initiation. With exception to the roughened sample, the category of ELM-induced damage for the pre-exposed samples is identical to the reference tests without pre-exposure to a particle flux.

PACS numbers: 28.52.Fa, 52.40.Hf, 52.55.Rk, 61.80.Fe, 61.80.Jh

1. Introduction

Currently, tungsten is considered as one of the few plasma-facing materials (PFMs) which is suitable for both current and next-generation fusion reactors. Tokamaks like JET and ASDEX Upgrade already use tungsten as PFM. The ITER-operation will start with a full tungsten divertor. Furthermore, also for future reactors, e.g. DEMO, tungsten will stay a promising PFM [1].

Despite the advantages of tungsten, e.g. low erosion rate, high melting point, and low tritium retention, there are also known drawbacks, e.g. plasma contamination and brittleness. During the operation of a fusion reactor, tungsten will be subjected to a combination of loading conditions, including neutron and particle irradiation, steady state heat fluxes, and transient heat fluxes. Each loading condition can damage tungsten, change the surface morphology, and modify the material properties [2, 3].

To investigate the influence of the different exposure conditions, tungsten was tested in several ways, e.g. by electron beam facilities or linear plasma devices. To study how each exposure condition affects the PFMs, various experiments focussed on one loading condition [4–6]. Although these experiments are necessary to understand the separate loads, the overall performance of tungsten as PFM could depend on the synergistic effects of the combined loads. For this reason, experiments were carried out in which tungsten was exposed simultaneously or successively to several exposure types [7–9].

An important interaction might occur between edge localized modes (ELMs), which lead to surface roughening, cracking, etc. [10], and steady state power and particle loading, which result in cavity formation, surface morphology modifications, etc. [11]. As a consequence, the thermal shock behaviour of tungsten that was exposed to H and He particles beforehand, performed at ITER relevant surface temperatures, needs to be understood and will be addressed hereafter.

2. Experimental set-up

The used material was cut from a 99.97 wt% pure tungsten disk with a height of ~ 45 mm and a radius of ~ 72 mm. This double-forged disk, characterized by a microstructure with elongated grains, was manufactured by Plansee. Three rectangular cuboid shapes, with a height of 5 mm for S-samples, 10 mm for M-samples, and 15 mm for L-samples, were chosen as sample geometry. Each surface of the samples was 5 mm by 10 mm. All samples were cut with a longitudinal grain-orientation. This means that the elongation of the grains is parallel to the surface. After polishing, the sample surfaces have a maximal arithmetic mean roughness (R_a) of 0.1 μm.

The exposure of the samples to a steady state particle and heat flux was done in the high heat flux facility GLADIS at the Max-Planck-Institut für Plasmaphysik [12]. A Gaussian beam was used that has a particle flux of $3.7 \times 10^{21}\,\mathrm{m^{-2}s^{-1}}$ at its centre. Through several 30 s long pulses, a total exposure time of 90 min was achieved, which corresponds to a fluence of $2 \times 10^{25}\,\mathrm{m^{-2}}$ at the beam maximum. The beam contained

either only H or a mixed H/He composition with 6% He. A 30 kV extraction voltage resulted for both cases in a heat flux of 10.5 MW/m^2 at the beam centre.

The energy distribution for the pure H beam is 35% H atoms of 10 keV, 43% H atoms of 15 keV and 22% H atoms of 30 keV, resulting in a mean particle energy of 17 keV. The assumption is made that the energy distribution of the H atoms in the mixed H/He beam is similar to the energy distribution of the pure H beam. Since spectroscopy only showed a Doppler shift from He^+, the He atoms have an energy of 30 keV [11]. The energy of the impinging particles in GLADIS is therefore much higher than the mean energy of the steady-state loading in a tokamak plasma, which is several 10 eV. While this could mean that the resulting damage is not the same, experiments have shown that the surface morphology changes due to incident He atoms can be similar for both energy ranges [13].

The samples were brazed upon an actively cooled CuCrZr structure. Therefore, the sample height determines the surface temperature during exposure. L-samples reached the highest temperatures, 1500°C. For M-samples, the surface temperature was 1000°C, while it was 600°C for S-samples. This results in six loading conditions for GLADIS, originating from two different particle beams on three sample-types.

ELM-like thermal loading was performed in the JUDITH 1 electron beam facility at Forschungszentrum Jülich [14, 15]. During each pulse, a focussed electron beam scans a square area measuring 4 mm by 4 mm on the sample surface for 1 ms. The loading spot moves on the surface with 47 kHz in the x-direction and 43 kHz in the y-direction. Each sample was exposed to 100 identical pulses, which have an absorbed power density of either 190 MW/m^2 (HFF-6) or 380 MW/m^2 (HFF-12), with a repetition rate of 0.5 Hz. A heater increased the sample temperature to 1000°C before the experiment started and kept it constant during the experiments. While the temperature of the bulk material was kept constant, the surface temperature in the loaded area rises during a pulse. For JUDITH 1, this results in two loading conditions.

At first, reference tests were performed with polished tungsten-samples. They were exposed to either the six GLADIS conditions or the two JUDITH 1 conditions. After obtaining these eight references, consecutive tests were executed. During these, pristine specimens were first exposed to GLADIS and thereafter in JUDITH 1, resulting in twelve different combinations. Due to a technical failure, the L-samples exposed in JUDITH 1 to HFF-6 could not be analysed. Post-mortem analysis of the thermal shock damage and the particle induced surface modifications was done with scanning electron microscopy (SEM), focussed ion beam (FIB), profilometry, and metallographic cross-sections.

3. Results and discussion

The GLADIS references are identical to the reference tests for earlier reported investigations of ELM-like damage at H or H/He exposed tungsten [16]. In all cases the sample surface was altered and an erosion pattern can be seen on SEM-pictures. Cross-sections of the L-samples showed grain growth up to ~ 3.5 mm deep, which did

Table 1. Arithmetic mean roughness R_a (μm) before thermal shocks, indicated by Pre-ELM, and after 100 thermal shocks at 1000°C, indicated by HFF-6 (190 MW/m^2) or HFF-12 (380 MW/m^2). The data is calculated from 50 points/mm profilometry.

Sample	Pre-ELM	HFF-6	HFF-12
Reference JUDITH 1	0.08	0.12	0.56
S-sample with H-flux	0.39	0.38	0.48
S-sample with H/He-flux	0.43	0.49	0.57
M-sample with H-flux	0.34	0.39	0.58
M-sample with H/He-flux	0.31	0.33	0.38
L-sample with H-flux	0.33	/	0.75
L-sample with H/He-flux	0.42	/	0.46

not happen for the S- and M-samples. While the average minimal and maximal Feret diameter of tungsten grains was 25 μm and 63 μm for the as-received material, it became for the L-samples 59 μm and 99 μm after GLADIS exposure. The M- and L-samples exposed to a H/He-flux also exhibit protruding surface structures. FIB-sections of the samples showed also cavities, as observed during other GLADIS-experiments [11].

Analyses of the reference JUDITH 1 samples indicate that there is no damage after HFF-6 for 1000°C base temperature. Such a lack of damage is in accordance with earlier results of HFF-6 on the same material at room temperature or 400°C [16]. For the reference HFF-12 at 1000°C, as shown in figure 1, the surface is heavily deformed and the R_a, shown in table 1, increases. The fine lines on the surface are either the beginning of crack formation or height differences on the surface. Both are present on the reference sample, but not enough data is available to determine an average crack depth. For example, crack initiations of around $\sim$ 300 nm depth are detected, as well as a crack which extends at least 6 μm deep, both shown in figure 1. These observations are in contrast with the damage behaviour at lower temperatures. After the HFF-12 pulses at temperatures where tungsten is ductile, only roughening occurs [10].

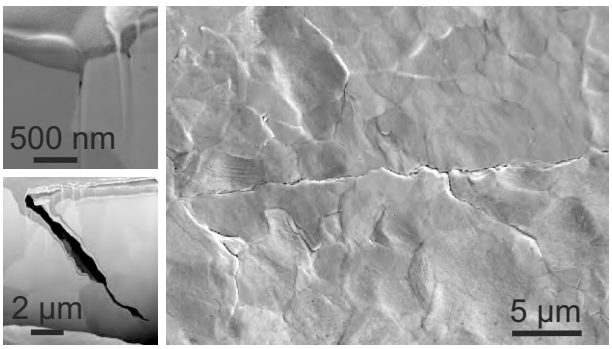

Figure 1. FIB-sections (left) and SEM (right) of pristine tungsten exposed to 100 pulses of HFF-12 at a base temperature of 1000°C.

Both SEM pictures and laser profilometry show no difference between GLADIS reference samples and the HFF-6 samples. Table 1 suggests an increased roughness

for the S-sample with H/He-exposure and the M-sample with H-exposure. However, the values differ by $\sim 0.05\,\mu$m from each other, which falls within the accuracy of the profilometry and is not considered a relevant increase. Metallographic cross-sections confirmed these conclusions. All post-mortem analyses show, similar to the JUDITH 1 reference, there is no damage after the low power density ELM-like loading.

The surface of each pre-exposed sample was altered after the HFF-12 ELM-like tests. This was either indicated by the R_a, see table 1, or by the SEM-pictures. For the L-sample with a pure H pre-exposure the damage was limited to surface roughening, while all the other samples also exhibited crack initiation. The increase of plasticity after recrystallization [17] is deemed to be responsible for the absence of crack initiation in this sample. Since no cracks were formed, the stress-relief in the near-surface layer during or after an ELM-like pulse can only happen by plastic deformation. For that reason, this sample is the only one with a substantial higher R_a than the reference sample.

The samples which show the beginning of crack formation are similar to the JUDITH 1 reference sample, e.g. figure 2. They have the same type of thin and shallow crack initiations. The average crack width gives a justification for the distinction between the crack network created during ELM-like tests at room temperature and the crack initiations created when the base temperature is kept at 1000°C. For a polished sample of the same tungsten grade, a crack network generated at HFF-12 at RT has an average crack width of $3.25\,\mu$m with a standard deviation of $1.32\,\mu$m. From the samples at a 1000°C base temperature during ELM-like tests, the highest average crack width of these crack initiations is $0.53\,\mu$m with a standard deviation of $0.39\,\mu$m, which was measured for the M-sample with H/He-exposure.

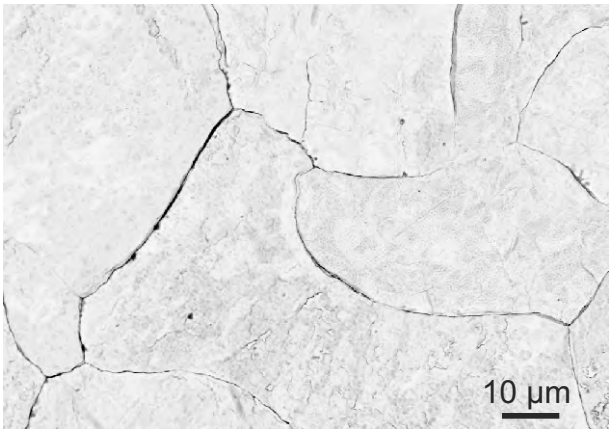

Figure 2. Tungsten surface of the M-sample with H exposure after 100 pulses of HFF-12 at a base temperature of 1000°C.

A comparison of the average crack width between all the samples with crack initiations shows that the lowest value is found for the JUDITH 1 reference sample. This polished sample without any pre-exposure, had crack initiations with an average width of $0.14\,\mu$m with a standard deviation of $0.05\,\mu$m. The other samples had an

average crack width between this $0.14\,\mu$m and the earlier mentioned $0.53\,\mu$m for the M-sample with H/He-exposure. Even while the average crack width is larger for the pre-exposed samples, these samples belong to the same damage category, namely crack initiations.

The observation of roughening and/or crack initiations at HFF-12 demonstrates that the power density where any form of damage starts to occur, i.e. the damage threshold, does not increase after H or H/He irradiation. In addition, the lack of any ELM-induced surface modifications at HFF-6 shows that the damage threshold does not decrease either.

FIB-sections on the H/He-exposed samples, e.g. figure 3, show that the shallow cracks are in the $0.3 - 6\,\mu$m range observed with the JUDITH 1 reference. The deepest measured crack on the FIB-sections is $\sim 5\,\mu$m, while the smallest crack depth measurement is $0.42\,\mu$m. Furthermore, after this analysis it is observed that for the S-sample exposed to the H/He beam, the cavities present in the subsurface layer are altered and have grown after the HFF-12 ELM-like loads at 1000°C base temperature.

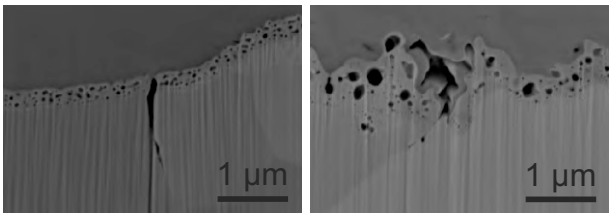

Figure 3. FIB-sections of the S-sample (left) and L-sample (right) with H/He-irradiation after HFF-12 pulses at a base temperature of 1000°C.

The cavities of the S-sample after HFF-12 ELM-like shocks are compared with two other samples using FIB-sections. The first sample used for comparing was the GLADIS reference sample with a surface temperature of 600°C during the H/He exposure. This sample did not undergo ELM-like thermal loads. The second sample, obtained from a previous experiment [16], that is used for comparing was a GLADIS sample with a surface temperature of 600°C during the H/He exposure, which underwent ELM-like thermal loads of HFF-12 in JUDITH 1 at room temperature. The FIB-analysis for the samples used in the comparison have similar cavities. Only the cavities of the mentioned S-sample with H/He-flux have changed.

This could be caused by heating up the base temperature to 1000°C for the duration of the experiments or it could be an effect of the thermal shocks at this temperature. While dedicated tests should be executed to pinpoint the cause, it is plausible to assume that the base temperature is a main factor. A potential explanation could be, if the cavity still contains gas, that even without a particle flux going to the material during the temperature rise, this could increase the gas pressure in the cavities. Furthermore, the shear modulus of tungsten decreases with increasing temperatures, reducing the required pressure for cavities growth according the Greenwood mechanical equilibrium condition [18, 19]. This might have resulted in cavity growth and explains why it only

happened for the S-sample.

Also on the metallographic cross-sections no deep crack propagations are observed, as figure 4 shows for H-exposed samples. The beginning of cracks in the micrometer range is not detectable in these cross-sections, due to their limited depth and size. This is another indication that the thermal shock behaviour is not deteriorated for the particle exposed samples, in comparison with the JUDITH 1 reference sample.

Figure 4. From left to right, the cross-section of the S-, M-, and L-samples with H-exposure after HFF-12 pulses at a base temperature of 1000°C.

4. Conclusion

The ELM-like tests on pristine material at 1000°C showed, as it is the case for experiments at lower temperatures, no damage at 190 $\mathrm{MW/m^2}$ ELM-like thermal loads, while damage occurs at 380 $\mathrm{MW/m^2}$ ELM-like thermal loads. The observed damage for the pristine material was not only surface roughening, but also the beginning of crack formation. These crack initiations at 1000°C differ from the crack networks at low base temperatures, since they do not form a large connected network, the average crack width is smaller and the crack initiations are more shallow than the cracks from samples with a crack network.

The material pre-exposed to a particle flux had a similar thermal shock behaviour. For one sample only surface roughening occurred which is a lower damage category than crack initiations, what happened to the pristine reference material. That sample does have a higher roughness parameter R_a, but that is not necessarily an indication of a worse damage behaviour after particle exposure. Especially since the difference in R_a before and after ELM-like thermal loads is still higher for the reference samples.

All the other samples with particle pre-exposure had just as the reference sample also shallow crack initiations. The R_a value of the samples with crack initiation, is not significantly higher than the R_a value of the reference sample. Also the crack depth of these crack initiations falls in the same range. Only one indication, the average crack width which is larger for pre-exposed samples, suggests that within the category of crack initiations the damage is more distinct.

Therefore, it is concluded that there is no degradation of the thermal shock behaviour, i.e. change of damage category, but only an indication of more pronounced

damage formation within the damage category. Potential effects of the crack width on the further development of damage needs to be addressed with higher pulse number experiments. In addition, this study found that the cavities of the H/He-exposed S-sample did grow after the JUDITH 1 exposure. Dedicated experiments will be necessary to resolve the responsible mechanism.

Acknowledgments

This work was supported by the European Commission and carried out within the framework of the Erasmus Mundus International Doctoral College in Fusion Science and Engineering (FUSION-DC). This work was executed under EUROfusion WP PFC. This work has been carried out within the framework of the EUROfusion Consortium and has received funding from the Euratom research and training programme 2014-2018 under grant agreement No 633053. The views and opinions expressed herein do not necessarily reflect those of the European Commission.

References

[1] Kaufmann M and Neu R 2007 *Fusion Engineering and Design* **82** 521–527
[2] Federici G, Skinner C H, Brooks J N, Coad J P, Grisolia C, Haasz A A, Hassanein A, Philipps V, Pitcher C S, Roth J, Wampler W R and Whyte D G 2001 *Nuclear Fusion* **41** 1967
[3] Philipps V 2011 *Journal of Nuclear Materials* **415** S2–S9
[4] Yoshida N, Iwakiri H, Tokunaga K and Baba T 2005 *Journal of Nuclear Materials* **337** 946–950
[5] Lemahieu N, Linke J, Pintsuk G, Van Oost G, Wirtz M and Zhou Z 2014 *Physica Scripta* **2014** 014035
[6] Yuan Y, Greuner H, Böswirth B, Krieger K, Luo G N, Xu H, Fu B, Li M and Liu W 2013 *Journal of Nuclear Materials* **433** 523–530
[7] Huber A, Wirtz M, Sergienko G, Steudel I, Arakcheev A, Burdakov A, Esser H G, Freisinger M, Kreter A, Linke J *et al.* 2015 *Fusion Engineering and Design* **in press**
[8] Loewenhoff T, Linke J, Pintsuk G, Pitts R and Riccardi B 2015 *Journal of Nuclear Materials* **463** 202–205
[9] van Eden G, Morgan T, van der Meiden H, Matejicek J, Chraska T, Wirtz M and Temmerman G D 2014 *Nuclear Fusion* **54** 123010
[10] Linke J, Loewenhoff T, Massaut V, Pintsuk G, Ritz G, Rödig M, Schmidt A, Thomser C, Uytdenhouwen I, Vasechko V and Wirtz M 2011 *Nuclear Fusion* **51** 6p
[11] Greuner H, Maier H, Balden M, Linsmeier C, Böswirth B, Lindig S, Norajitra P, Antusch S and Rieth M 2013 *Journal of Nuclear Materials* **442** S256–S260
[12] Greuner H, Boeswirth B, Boscary J and McNeely P 2007 *Journal of Nuclear Materials* **367** 1444–1448
[13] Wright G, Brunner D, Baldwin M, Doerner R, Labombard B, Lipschultz B, Terry J and Whyte D 2012 *Nuclear Fusion* **52** 042003
[14] Duwe R, Kühnlein W and Münstermann H 1994 *Fusion Technology* 355–358
[15] Linke J, Bolt H, Duwe R, Kühnlein W, Lodato A, Rödig M, Schöpflin K and Wiechers B 2000 *Journal of Nuclear Materials* **283–287** 1152–1156
[16] Lemahieu N, Greuner H, Linke J, Maier H, Pintsuk G, Van Oost G and Wirtz M 2015 *Fusion Engineering and Design* **In press**
[17] Wirtz M, Cempura G, Linke J, Pintsuk G and Uytdenhouwen I 2013 *Fusion Engineering and Design* **88** 1768–1772

[18] Greenwood G, Foreman A and Rimmer D 1959 *Journal of Nuclear Materials* **1** 305–324
[19] Sang C, Sun J, Bonnin X, Liu S and Wang D 2013 *Journal of Nuclear Materials* **443** 403–408